LA-9054-MS

C.3

Numerical Modeling of Gun Experiments
with Impact Velocities
Near the SDT Threshold

Thermal Explosion Initiated by Friction Heat

# Los Alamos
Los Alamos National Laboratory
Los Alamos, New Mexico 87545

# Numerical Modeling of Gun Experiments with Impact Velocities Less Than SDT Threshold

## Thermal Explosion Initiated by Friction Heat

W. D. Barfield

# Los Alamos

Los Alamos National Laboratory
Los Alamos, New Mexico 87545

# NUMERICAL MODELING OF GUN EXPERIMENTS WITH IMPACT VELOCITIES LESS THAN SDT THRESHOLD

## THERMAL EXPLOSION INITIATED BY FRICTION HEAT[*]

by

W. D. Barfield

## ABSTRACT

One- and two-dimensional calculations have been made to model thermal explosion ignited by friction heat, hypothesized as an initiation mechanism for the unknown XDT phenomenon that is responsible for detonations observed in gun experiments with impact velocities less than threshold for shock-to-detonation transition. Preliminary results reported here suggest that friction-induced thermal explosion would be quenched by cooling associated with side rarefactions after penetrating only a thin layer of the propellant. Other effects (not modeled here) would be expected to increase the calculated heating rates or speed up the friction-induced thermal explosion. For this reason, friction cannot be ruled out as an initiation mechanism on the basis of the results described here.

---

I.  INTRODUCTION

In gun experiments a cylindrical projectile of the propellant under investigation is fired at a heavy target, usually steel. The tests show significant probability of high-level detonation at impact velocities that are below the threshold for shock-to-detonation transition (SDT)[1] (see Table I). Because the process by which such detonations take place is not understood, it has been called XDT. The phenomenon is further characterized by detonation delays from 2 to 10 times longer than those for SDT in the same test. Similar detonations have been observed in other types of experiments involving low-velocity impacts.

---

[*]Interim results as of March 1981; work still in progress.

1

TABLE I

TRANSITION THRESHOLDS
(mm/μs)

| | Projectile Diameter (mm) | | | |
|---|---|---|---|---|
| | 18 | 25 | 70 | 155 |
| SDT | 0.73[a,b] | 0.71[a] <br> >0.8[c] | 0.69[c] | 0.54[c] |
| XDT | 0.36[b] | 0.48[a] | 0.33[a] <br> 0.28 - 0.31e | 0.27[d,e] |

[a]"Trident-I (C-4) Final Report for FY 80, Detonation Modeling Support Study," Hercules-Thiokol (December 1980).

[b]R. C. Jensen, et al. (Hercules Inc.), 7th Symposium (International) on Detonation, Annapolis (1981).

[c]Estimated Value computed using (extrapolated) normal density "Pop plot" with run = 0.5 diam, shock-material velocity relations, and shock relations (neglecting material strength).

[d]"High Energy Propellant Safety, Informal Progress Report," Lawrence Livermore Laboratory report UCID-17272-80-3 (September 1980), p. 15.

[e]"High Energy Propellant Safety, Informal Progress Report," Lawrence Livermore Laboratory report UCID-17272-80-1 (January 1980), pp. 62 and 64.

This report describes modeling of thermal explosion initiated by friction heat, hypothesized as an initiation mechanism for XDT.

## II. CALCULATIONAL MODEL

To model the gun experiments, the two-dimensional, Lagrangian hydrodynamics, elastic-plastic flow code TDL[1] was modified to incorporate friction drag forces and associated heating along a slip surface, representing the explosive/ steel interface. New boundary conditions for free surfaces and for the heat conduction equation were also added.

At free surfaces the normal stress and shear stress are set to zero; the tangential stress is determined by the difference equation that holds within the material:

$$\sigma_{nn} = \sigma_{n\tau} = 0 \quad ,$$

$$\sigma_{\tau\tau} \text{ (no boundary condition)} \quad .$$

A radiation boundary condition is used for the heat conduction equation

$$\nabla T = AT \quad (A = \text{constant}) \quad .$$

At a slip surface the normal and shear stresses are continuous, and the tangential stress is again determined by the difference equations within the separate materials:

$$\left. \begin{array}{c} \sigma_{nn} \\ \\ \sigma_{n\tau} \end{array} \right\} \text{ continuous}$$

$$\sigma_{\tau\tau} \quad \text{(no jump condition)} \quad .$$

In case $\sigma_{nn} < 0$ on both sides (tension), the surfaces are allowed to separate (free surface boundary conditions). Separation is also allowed if a gap forms that is larger than 0.1 times the cell dimension. After separation the positions of the surfaces are monitored to allow for possible reclosure. Continuity of temperature and heat flux are ensured by setting

$$\left\langle \frac{K}{\Delta N} \right\rangle = \frac{2(K_1/\Delta n_1)(K_2/\Delta n_2)}{(K_1/\Delta n_1) + (K_2/\Delta n_2)}$$

at a material interface. (K = thermal conductivity, and $\Delta n$ = cell dimension normal to interface.) The normal and tangential components of the stress deviators $S_{ij}^{*'}$ are related to the usual x,z components S by

---

$S_{xx}^{*} = P - \sigma_{xx}$, $S_{zz} = P - \sigma_{zz}$, and $S_{xz} = \sigma_{xz}$.

$$S'_{ij} = \sum_k \sum_\ell R_i^k R_j^\ell S_{k\ell} \quad (i,j = n,\tau \quad, \quad k,\ell = x,z) \quad,$$

or, in matrix notation,

$$S' = RSR^T \quad,$$

where R rotates the coordinate frame through an angle $\theta$ (See Fig. 1):

$$R = \begin{pmatrix} \cos\theta & \sin\theta \\ -\sin\theta & \cos\theta \end{pmatrix} \quad.$$

This gives

$$S_{nn} = S_{xx} \cos^2\theta + S_{zz} \sin^2\theta + 2S_{xz} \cos\theta \sin\theta$$

$$S_{\tau n} = S_{xz}(\cos^2\theta - \sin^2\theta) - (S_{xx} - S_{zz}) \cos\theta \sin\theta$$

$$S_{\tau\tau} = S_{xx} \sin^2\theta + S_{zz} \cos^2\theta - 2S_{xz} \cos\theta \sin\theta \quad,$$

where $\theta$ = angle of rotation (angle between surface normal and x-axis). Points on the surface have normal and tangential accelerations.[*]

$$a_n = V\left[ -\frac{\partial\sigma_{nn}}{\partial n} + \frac{\partial\sigma_{\tau n}}{\partial\tau} \right] \quad,$$

$$a_\tau = V\left[ -\frac{\partial\sigma_{\tau\tau}}{\partial\tau} + \frac{\partial\sigma_{\tau n}}{\partial n} \right] \quad, \text{ and}$$

$$a_x = a_n \cos\theta - a_\tau \sin\theta \quad,$$

$$a_z = a_n \sin\theta + a_\tau \cos\theta \quad.$$

---

[*]The x,y difference equations cannot be applied across the slip interface because of the jump in $\sigma_{\tau\tau}$.
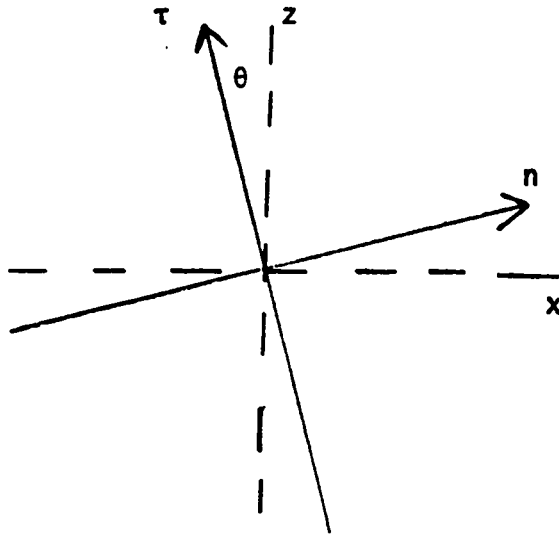
Fig. 1.
Rotation of coordinate frame.

The friction drag force is incorporated by setting

$$\sigma_{\tau n} = \$\mu\sigma_{nn}$$

at the slip interface* [$\mu$ = friction coefficient, and $\$$ = sign of relative tangential velocity $\Delta u_\tau = u_\tau^{(1)} - u_\tau^{(2)}$]. Note that $\sigma_{\tau n}$ is continuous at the interface, as required by boundary conditions. The friction heat flux = work done by drag force = $\mu\sigma_{nn}|\Delta u_\tau|$, part of which flows into each material. Heat flux partitioning at the interface is determined by the thermal properties of the two materials. An approximate expression for the partitioning is derived in Appendix A.

---

*This is equivalent to averaging over localized friction hot spots at points of contact on the surfaces. Anderson[2] reviewed the friction hot-spot phenomenology and developed an approximate expression for the friction coefficient of a material in terms of the "parameters that control the friction shear. The results were used in conjunction with the frictional heating equations and thermal decomposition kinetics to discuss the factors that control the sensitivity of explosive materials to frictional heating under various conditions. The predicted effects are in good qualitative agreement with known experimental evidence. On a more quantitative basis, however, it was shown that the processes involved can be quite complex. It is evident that the more closely the frictional initiation event is examined, the more closely one arrives at the proverbial can of worms."

# III. THERMAL EXPLOSION INITIATED BY FRICTION HEAT

Two-dimensional calculations were done to obtain an estimate of the friction heat flux at the interface in the gun experiments and to study the effects of side rarefactions. Figure 2a shows the calculated configuration at 10 µs after impact for the 70-mm gun, where a 72-mm-diam by 76-mm cylinder of VRP with 0.5-mm/µs initial velocity impacts a steel block. [Because the slip surface in the TDL code is initially at R = constant, the experimental configuration was approximated by semi-infinite slabs (x-z geometry),[*] with $\Delta x = \Delta z =$ 4-mm cells.] Figures 2b, c, d, and e also show velocity vectors and contours of z-velocity and temperatures. The smaller "Shotgun" test (36-mm-diam by 18-mm projectile) was also modeled. Table II gives material properties used for VRP and steel.[**] Table III gives the calculated friction-heat fluxes into selected VRP cells along the interface. The calculations were terminated when the corner cells became highly deformed.

---

[*]Results of cylindrical geometry calculations are described in the addendum.

[**]Melting was not allowed. An approximate expression for variation of melting point with pressure, $\Delta T(K) = 20\ \Delta P(KB)$, quoted in Ref. 2, suggests that, at the impact stresses occurring in the calculations reported here, it is likely that melting does not occur. There is some evidence that a viscoelastic model might give a better description of VRP than an elastic-plastic model can give.
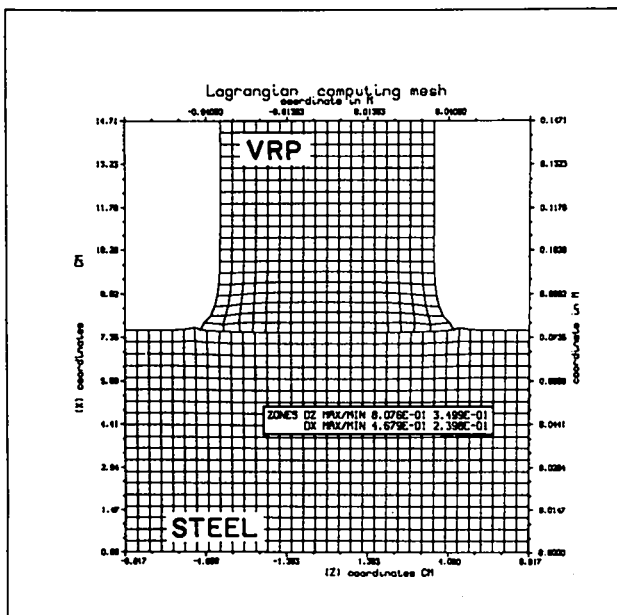


Fig. 2a.
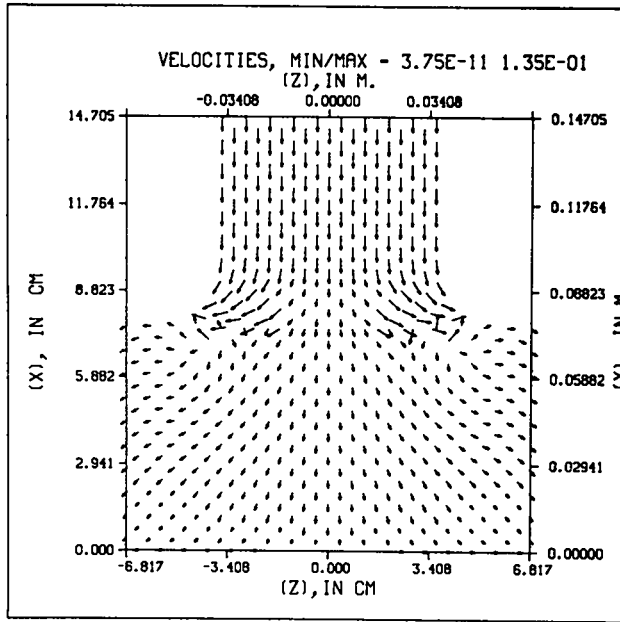Calculated configuration of 70-mm gun experiment at 10 µs. Initial velocity (VRP) $u_{x0} = -0.5$ mm/µs.
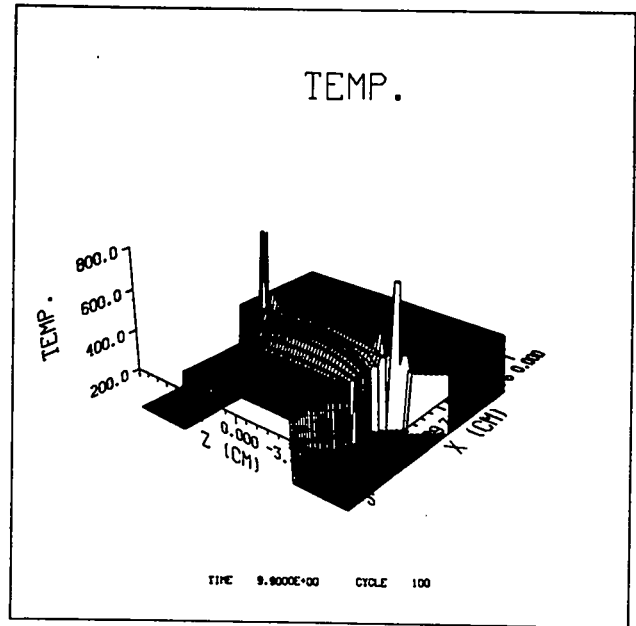
**Fig. 2b.**
Velocity vectors (logarithmic length
scale).



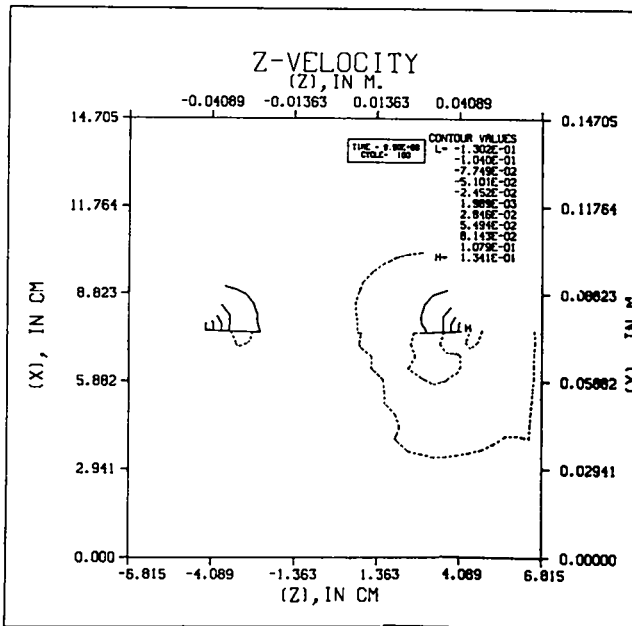**Fig. 2c.**
Temperature perspective plot.



**Fig. 2d.**



**Fig. 2e.**

Z-velocity (cm/µs) contours at 10 and 15 µs. The coefficient of friction was set
to zero after 1.2 µs. The steel cells opposite the projectile corners are in ten-
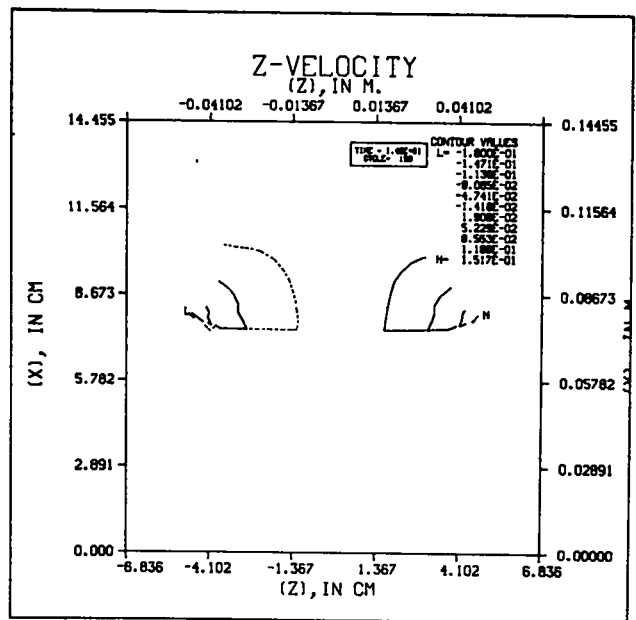sion and are significantly hotter than surrounding cells.

## TABLE II

## MATERIAL CONSTANTS USED IN CALCULATIONS

### HOM Equation of State Parameters[a]

#### Steel

| | | | |
|---|---|---|---|
| C | 4.58000000000E-01 | CV | 1.07000000000E-01 |
| S | 1.51000000000E+00 | V0 | 1.26310471100E-01 |
| F | -3.82382587453E+03 | α | 1.17000000000E-05 |
| G | -7.03211954024E+03 | SFA | 0.0 |
| H | -4.82670213890E+03 | USP | 1.25000000000E-01 |
| I | -1.46678402118E+03 | μ | 9.87000000000E-01 |
| J | -1.66391615983E+02 | Y0 | 7.50000000000E-03 |
| Y | 2.00000000000E+00 | FLAF | 5.00000000000E-02 |

#### VRP

| | | | |
|---|---|---|---|
| C | 1.99000000000E-01 | C | 3.18097259766E-01 |
| S | 2.00000000000E+00 | D | -3.94574700710E-02 |
| F | -5.40502394255E+00 | E | 1.86437978542E-03 |
| G | -4.86025889997E+01 | K | -1.57124113947E+00 |
| H | -7.54072015339E+01 | L | 5.35136520243E-01 |
| I | -4.59699218022E+01 | M | 7.67136706803E-02 |
| J | -6.62503957745E+00 | N | 5.76342096779E-03 |
| Y | 1.50000000000E+00 | O | 1.60356885887E-04 |
| CV | 3.00000000000E-01 | P | 7.96340485711E+00 |
| V0 | 5.44662309368E-01 | R | -4.82226700328E-01 |
| α | 1.63000000000E-04 | S | 1.20767297198E-01 |
| μ | 5.00000000000E-02 | T | -1.70230990191E-02 |
| Y0 | 5.00000000000E-04 | U | 8.86138770815E-04 |
| FLAF | 1.00000000000E-02 | CV' | 5.00000000000E-01 |
| A | -3.56380388220E+00 | Z | 1.00000000000E-01 |
| B | -2.30435144510E+00 | | |

| Thermal Conductivity | Arrhenius Burn Parameters for VRO[c] | |
|---|---|---|
| Steel - K = 0.1 cal/cm·s·K | Activation energy (kcal/mole) | 36.5 |
| VRP[b] - K = 0.001 cal/cm·s·K | Collision frequency (s$^{-1}$) | $3.6 \times 10^{16}$ |

### Coefficient of Friction

$\mu = 1.0$

[a]For V in $cm^3$/g, P in Mbar, I in Mbar·$cm^3$/g, T in K, CV in cal/g·K (Ref. 1).

[b]Gibbs and Popolato (1980). The same value was used for solid and gas. Power-law extrapolation of conductivity measurements for steam/$N_2$ mixture given in Touloukian et al. (1970) to 3000 K gives a value within 25% of the value used for unburned VRP.

[c]R. N. Rogers, Los Alamos National Laboratory. The VRO values were used for VRP in the calculations reported here.

TABLE III

CALCULATED HEAT FLUXES

| | Cycle | Time (µs) | Friction Heat into VRP $(10^{-6}$ Mbar-cm$^3$/cm$^2$-µs$)^a$ | | |
| | | | Outside | Halfway | Center |
| Shotgun | 10 | 0.8 | 9.5 | 2.8 | 0 |
| | 20 | 1.6 | 7.6 | 6.8 | 6.2 |
| | 30 | 2.4 | 2.8 | 4.7 | 6.0 |
| | 40 | 3.2 | 1.0 | 1.9 | 4.5 |
| 70-mm Gun$^b$ | 10 | 1.0 | 25.0 | 0 | 0 |

$^a 10^6$ Mbar-cm$^3 \cong 0.024$ cal.

$^b$Friction coefficient set at zero after 1.2 µs.

The resolution of the 2-D calculations is too crude to follow the penetration of a possible friction heat-induced burn wave into the explosive. For this reason fine-zoned 1-D calculations representing a slice perpendicular to the interface were carried out, and the friction heat fluxes into VRP and steel from the 2-D calculations were included as heat sources in the cells adjacent to the interface. Two cases were computed: (1) $\Delta x_0 = 10$ µm, no heat conduction (1D-1), and (2) $\Delta x_0 = 0.1$ µm, heat conduction (1D-2). In both cases the friction heat fluxes were taken to be $6.4 \times 10^{-5}$ (into steel), $5 \times 10^{-6}$ Mbar·cm$^3$/cm$^2$·µs (VRP). In problem 1D-1 the temperature of the first VRP zone (adjacent to steel) rises steadily, reaching ~750 K at about 1.2 µs, at which temperature the zone burns, leaving detonation products at about 3000 K (Fig. 3). The temperature of the second VRP zone increased to about 485 K at about 1.2 µs, remaining constant until the calculation was terminated at ~1.45 µs. Figure 4 shows the shocks associated with the expansion of the burned zone.

Problem 1D-2 studied heat conduction as a mechanism for transferring energy from the burned cell.$^*$ Results show a behavior similar to 1D-1, except that the

---

$^*$The steep thermal gradients (see Appendix B) are not resolved in a calculation with $\Delta x = 10$ µm, where the largest gradient that can be represented is $\cong$ (0.001 cal/cm·s·K) (2500 K)/0.001 cm $\cong$ 2.5 kcal/cm$^2$·s.
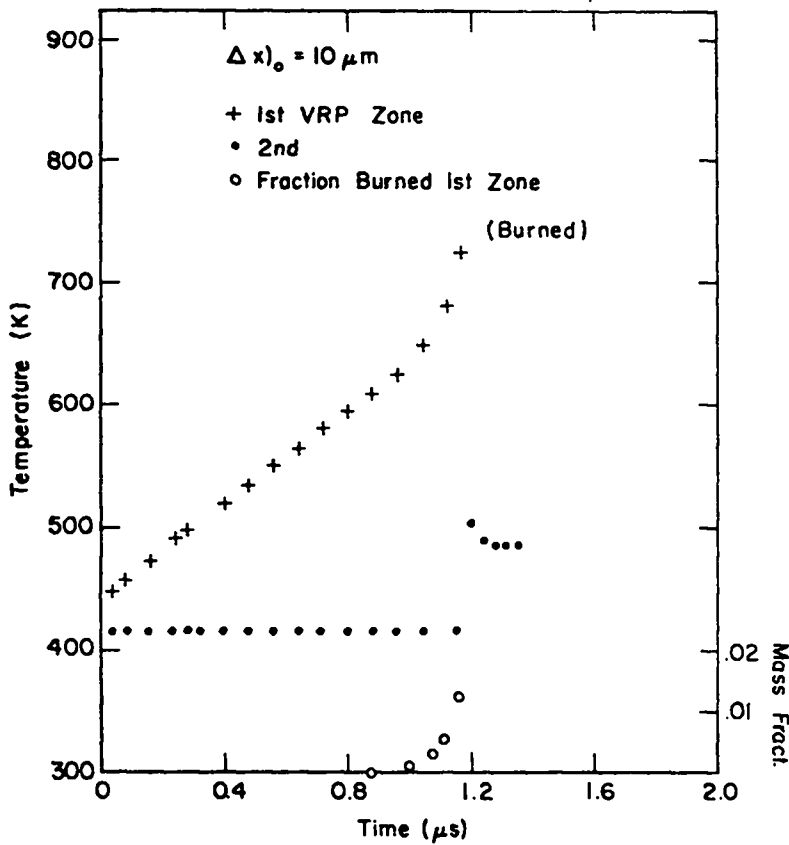
Fig. 3.
Temperature and mass fraction of decomposed VRP histories for first two zones, problem 1D-1. After the first zone burned completely, its temperature was approximately 3000 K.
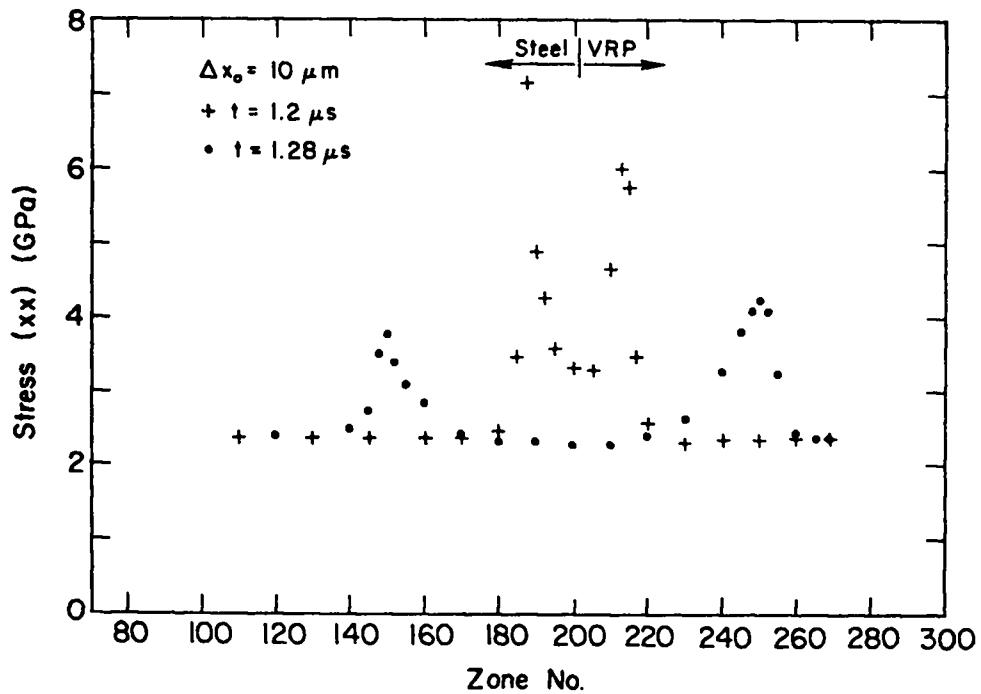


Fig. 4.
Stress ($\sigma_{xx}$) profiles, problem 1D-1, at 1.2 and 1.28 μs. The plot shows the shocks associated with expansion of the burned zone (No. 201). Only a portion of the mesh points is plotted.

time scale is compressed (see Fig. 5). In this case the temperature of the second VRP zone increases until the time (21 ns) the calculation was terminated. (The shock associated with the expansion of the burned zone had run through all the zones available.) Although it is not clear what a 1-D calculation means on this scale,[*] the results suggest that heat conduction may furnish the required energy transfer mechanism to enable the reaction to propagate into VRP.

Approximate analytical solutions of the heat conduction equation (Appendix B) were used to continue the 1-D numerical calculations. Figures 6-8 show the temperature of the second VRP zone for 1D-1 and 1D-2 as given by the analytical solutions.[**] Problem 1D-1 was also continued numerically by (1) turning off the hydrodynamics (that is, setting material velocities to zero) and friction heat flux at the interface at cycle 3300 (t = 1.32 $\mu$s), when the shock associated with the expansion of the VRP zone on burning had run through the available zones; (2) turning on heat conduction; and (3) increasing the time integration step[†] from 0.4 ns to 1.0 $\mu$s. Figure 9 gives the calculated temperature and burn history of the second zone (compare Fig. 6); these results suggest that the friction-induced thermal explosion "goes," although penetrating VRP at a rather slow rate, in semi-infinite slab geometry (no side rarefactions). In problem 1D-1 the initial velocity of penetration at a depth of 20 to 30 $\mu$m is (Fig. 6)

$$\frac{dx}{dt} \cong \frac{10 \ \mu m}{80 \ \mu s} \cong 0.1 \ m/s.$$

For problem 1D-2 the initial velocity at penetration depth of 0.2 to 0.3 $\mu$m is (Fig. 7)

$$\frac{dx}{dt} \cong \frac{0.1 \ \mu m}{0.008 \ \mu s} \cong 10 \ m/s \quad .$$

---

[*]The surface asperities responsible for friction have dimensions 0.1-0.5 $\mu$m (Ref. 3).

[**]In Figs. 6-8 the zero of time is taken as time of first zone burn. In the analytical solution the second zone was assumed to start from 460 K at the time of first zone burn. It would have been better to use 490 K, as in Fig. 3.

[†]The Courant condition for the hydrodynamics restricted $\Delta t$ to the smaller value.
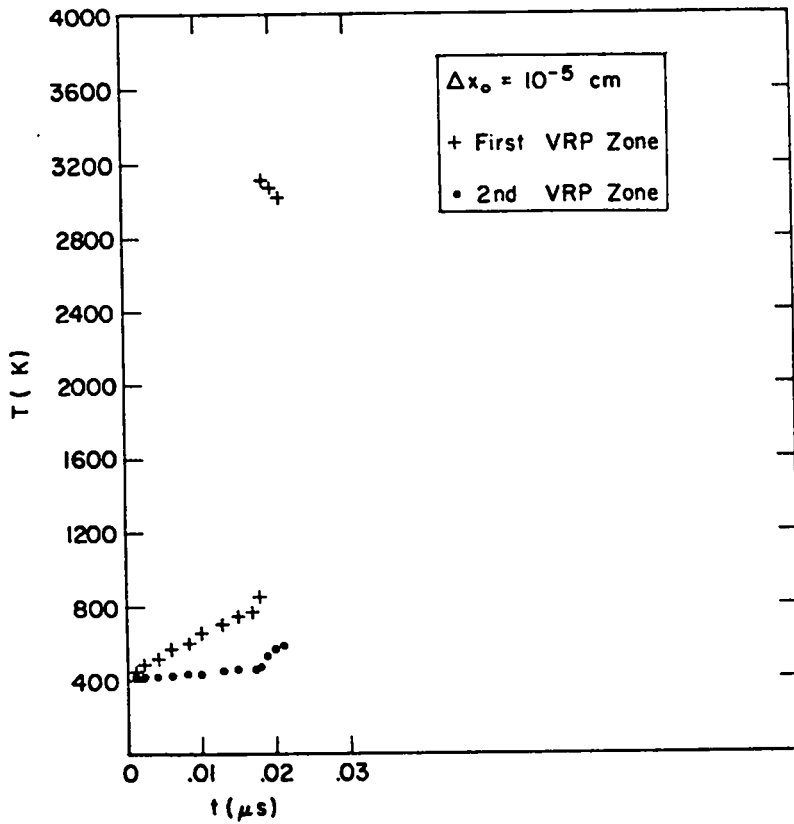
Fig. 5.
Temperature histories of first two VRP zones, problem 1D-2.
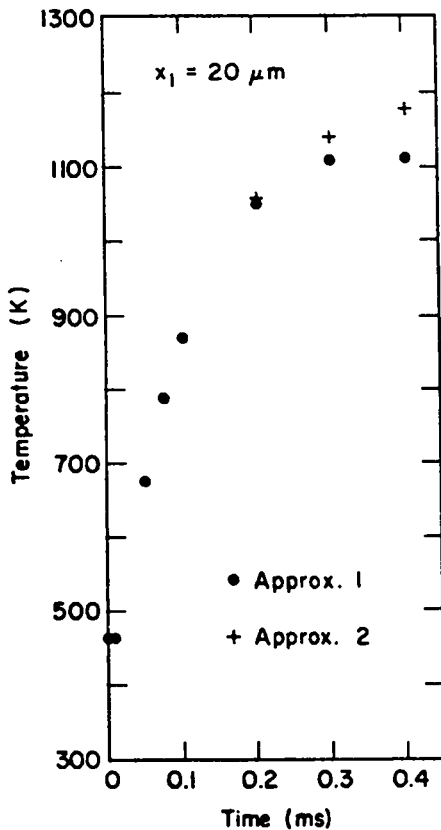


Fig. 6.
Temperature history of second VRP zone (x = 25 μm), problem 1D-1, calculated by two different approximate analytical solutions of the heat conduction equation. The zero of the time scale corresponds to time of first zone burn (~1.18 μs) (Fig. 3).
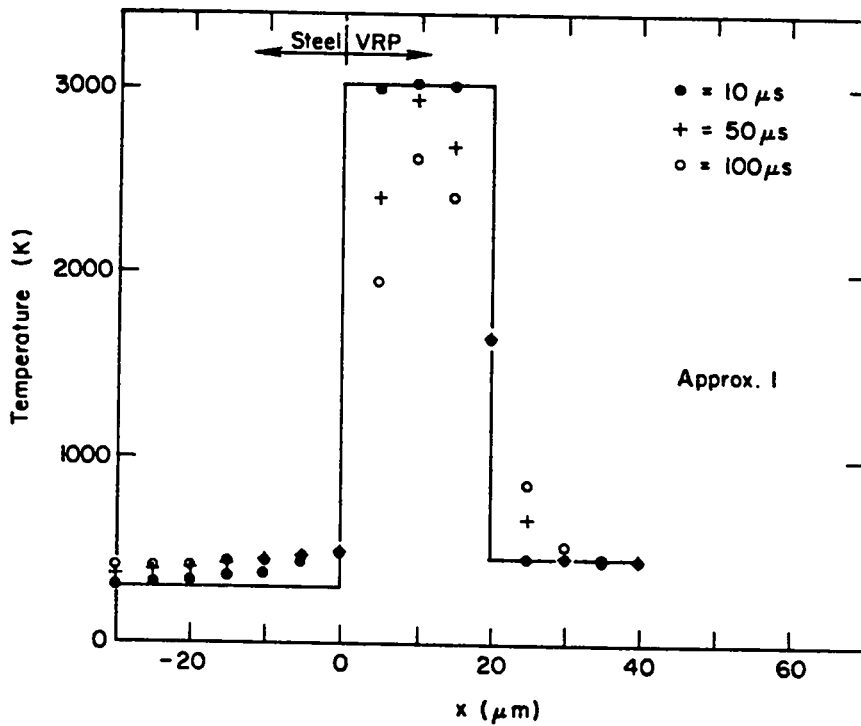
12

**Fig. 7.**
Temperature profiles, approximate analytical solution, problem 1D-1, at three times after time of first zone burn.



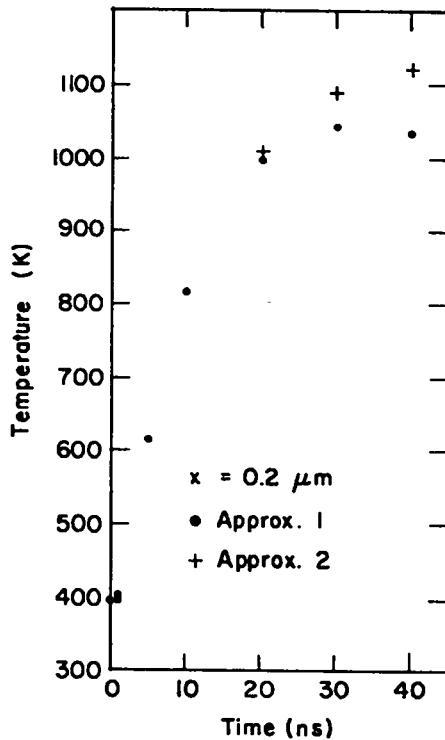**Fig. 8.**
Temperature history of second VRP zone (x = 0.25 μm), problem 1D-2, as calculated by two different approximate analytical solutions of heat conduction equation. The zero of the time scale corresponds to time of first zone burn (~18.5 ns) (Fig. 5).
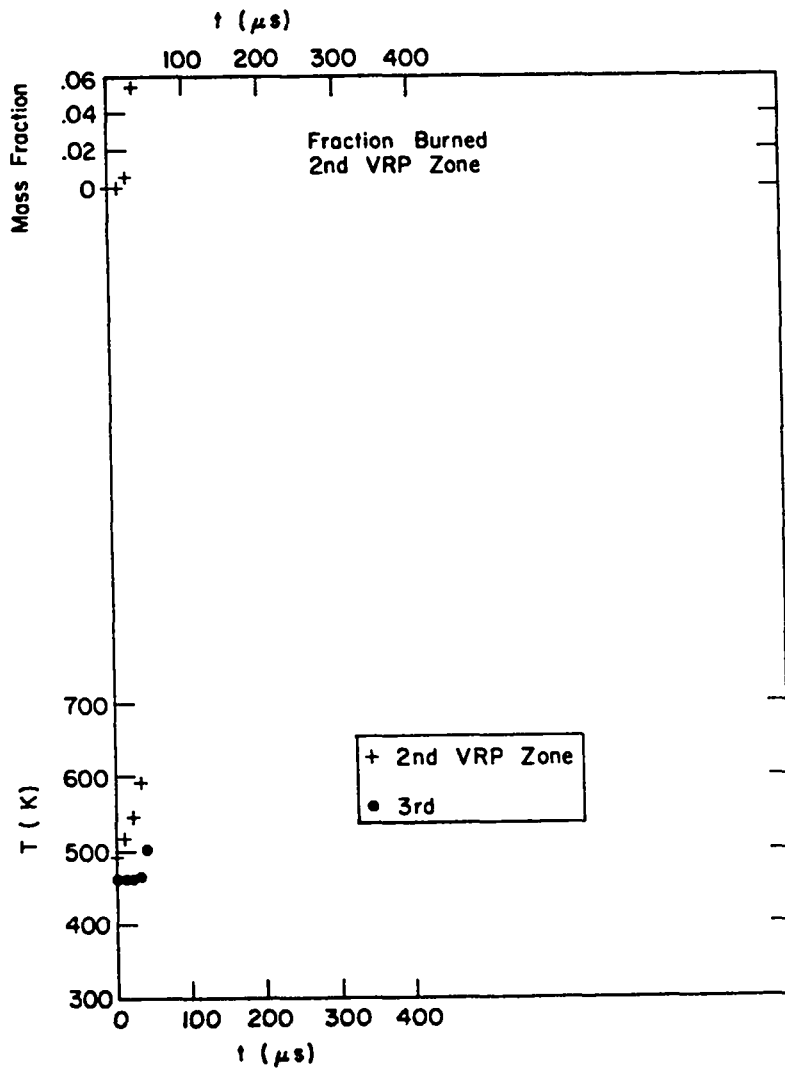
Fig. 9.
Temperature and mass fraction of decomposed VRP histories for second and third VRP zones, problem 1D-1, continued numerically without hydrodynamic motion. (Compare Fig. 6.)

The heating rate caused by heat conduction in Figs. 6, 8, and 9 can be compared with expansion cooling rates associated with side rarefactions as given by the 2-D calculations (Fig. 2d and e, Table IV).[*]

---

[*]The heating rate attributed to friction in the 2-D calculations is small because friction heating is confined to a thin layer (a small fraction of cell dimension) adjacent to the interface.
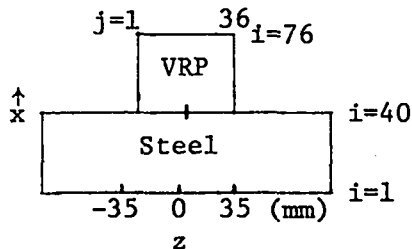
TABLE IV

HEATING RATES (K/$\mu$s)
($u_0$ = -0.5 mm/$\mu$s)

| t ($\mu$s) | 1-D Analytical Solution[a] | $(-PdV/dt)/c_v$ Cell (40,2)[b] | Cell (40,10) | Shear Heat Rate[c] Cell (40,2) | Cell (40,10) |
|---|---|---|---|---|---|
| 0.8 | | +261 | +272 | 0.08 | $4 \times 10^{-8}$ |
| 2.4 | | -17.5 | +4 | 0.001 | 0.002 |
| 3.6 | | +2.5 | 0 | | |
| 4.4 | | +22.5 | -1.2 | 0.33 | -0.001 |
| 5.6 | | -21 | -2.5 | 0.25 | 0.002 |
| 7.2 | | -7 | -4 | 0.08 | 0.002 |
| 8.4 | | | -2.5 | 0.7 | 0.004 |
| 9.2 | | | -5.0 | 0.5 | 0.004 |
| 9.8 | | | -5.0 | | |
| 10-50 | $\sim$+5 | | | | |
| 50-75 | $\sim$4 | | | | |
| 75-100 | $\sim$3 | | | | |

[a]Fig. 6, 2nd VRP zone. Rate due to heat conduction (0.02 < x < 0.03 mm).
[b](40,2): first row of VRP cells (-33 < z < -31 mm).
(40,10): first row of VRP cells (-17 < z < -15 mm).



[c]Shear heat rate = $c_v^{-1} V \sigma_{xz} \left( \dfrac{\partial u_x}{\partial z} + \dfrac{\partial u_z}{\partial x} \right)$ .

## IV. SUMMARY

One- and two-dimensional numerical calculations in slab geometry have been used to model thermal explosion induced by friction heat at the projectile/target interface as an initiation mechanism for the detonations observed in gun experiments at impact velocities less than SDT threshold. Because of the greatly

different scales (space and time) for hydrodynamic motions and heat conduction, it has not been possible to include both in a single 2-D calculation.

Results of 1-D calculations of the penetration of a thermal explosion (that is, propagated by heat conduction) initiated by a friction heat source (from 2-D calculations) suggest that the explosion propagates perpendicular to the interface at a rather slow rate (of the order of meters/second) in semi-infinite slab geometry (no side rarefactions). Results of the 2-D calculations given in Table IV indicate that cooling by side rarefactions would quickly quench (in less than 10 μs) such a thermal explosion in the absence of other effects (not modeled here) that would be expected to increase the heating rates or speed up the friction-induced thermal explosion. These might include (1) shock-induced decomposition;* (2) enhancement of shock reflected from the target by overtaking shock from the thermal explosion (Fig. 4), which would tend to make the "Forest Fire" burn at a higher rate; (3) shock damage to propellant** increasing its sensitivity; (4) propagation of thermal explosion into resulting cracks in propellant;** and (5) possible orders-of-magnitude shock enhancement of thermal conductivity.[4] Thus, friction cannot be ruled out as an initiating mechanism for XDT on the basis of the results reported here.

ACKNOWLEDGMENTS

---

* "Forest Fire" burn,[1] suggested by C. A. Forest, Los Alamos National Laboratory.
** This information supplied by A. L. Bowman, Los Alamos National Laboratory.

ADDENDUM
(December 1981)

## RESULTS OF CYLINDRICAL GEOMETRY CALCULATIONS;
## EFFECT OF ENHANCED THERMAL CONDUCTIVITY

By switching the roles of R and Z so that Z = 0 becomes the axis of cylin-
drical symmetry, a version of the TDL code was constructed that permits a plane
initially perpendicular to the axis of symmetry to be a slip surface. The modi-
fied version was used to model the Shotgun and 70-mm gun experiments in cylin-
drical geometry.

Results for friction heat flux into VRP are compared with the slab geometry
approximation results (from Table III) in Table AD-I. The fluxes calculated in
cylindrical geometry are significantly smaller near the outer radius than the
values calculated in slab geometry.

Compressive heating rates (Table AD-II) can be compared with the slab ge-
ometry values of Table IV. By 15 μs the cooling of the first row of VRP cells
by the rarefaction is essentially over. This suggests that the conclusion
reached on the basis of slab geometry calculations--that is, that the thermal
explosion is quenched by the rarefaction--may be wrong. (Note from column 2 of
Table IV that the thermal explosion is just getting started at 15 μs after im-
pact.) Figures AD-1 and AD-2 show temperature and radial (z) velocity contours[*]
at 15 μs. Figure AD-3 is a perspective plot of radial velocity. In any case,
it is clear from the 1-D results that only a very thin layer of propellant is
penetrated by the thermal explosion in times of interest for XDT.

The effect of an enhanced thermal conductivity[4] on the propagation of the
thermal explosion was estimated by comparing two approximate 1-D slab geometry
analytical solutions of the heat flow equation (Fig. AD-4). In the enhanced
conductivity case the temperature of the unburned propellant does not rise above
510 K.

---

[*]The temperature profile produced by friction heat (that is, the thermal explo-
sion) is not resolved by the coarse 2-D mesh. It is confined to a very thin
layer adjacent to the interface.

## TABLE AD-I

### FRICTION HEAT INTO VRP[a]

$$(10^{-6}\ \text{Mbar-cm}^3/\text{cm}^2\text{-}\mu s)$$

| | Time ($\mu s$) | Outside | Halfway | Center |
|---|---|---|---|---|
| Shotgun (slab geometry) | 0.8 | 9.5 | 2.8 | 0. |
| | 1.6 | 7.6 | 6.8 | 6.2 |
| | 2.4 | 2.8 | 4.7 | 4.0 |
| | 3.2 | 1.0 | 1.9 | 4.5 |
| Shotgun (cylinder) | 2.0 | 1.0 | 1.5 | >0.2 |
| | 4.0 | 0.5 | 0.4 | 0.7 |
| 70-mm gun (slab geometry) | 1.0 | 25.0 | 0. | 0. |
| 70-mm gun (cylinder) | 0.8 | 6.6 | 35. | 7.2 |

[a] $u_0 = 0.05$ cm/$\mu s$, $\mu = 1.0$. The friction coefficient was set = 0 after 1.2 $\mu s$ in the 70-mm gun calculations. $10^{-6}$ Mbar-cm$^3 \cong 0.1$ joule.


## TABLE AD-II

### COMPRESSIVE HEATING RATES[a]

$$-c_v^{-1}(P + Q)\ dV/dt\ (K/\mu s)$$

| t ($\mu s$) | Axis | 1.2 < R < 1.6 cm | Next-to-Outside Cell |
|---|---|---|---|
| 0.8 | +51. | +60. | +47. |
| 1.8 | +30. | +51. | +31. |
| 4.8 | +1.5 | -2.7 | -13. |
| 9.8 | -0.4 | -7.4 | -0.8 |
| 14.8 | -4.0 | -2.1 | +1.0 |

[a] First row of VRP cells, cylindrical geometry, 70-mm gun. $u_0 = 0.05$ cm/$\mu s$.
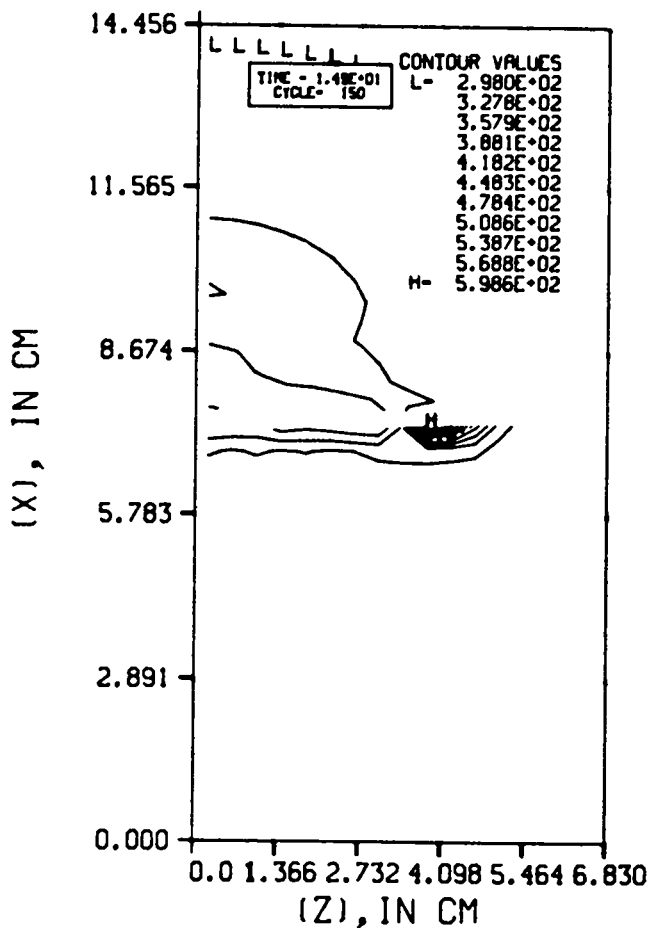
## TEMP.



Fig. AD-1.
Temperature contours (K) at 15 μs after
impact for 70-mm gun experiment simula-
tion calculated with cylindrical geome-
try version of TDL code. The interface
was initially at x = 7.6 cm; Z = radial
coordinate. Limited velocity (VRP) =
0.05 cm/μs. μ = friction coefficient =
1.0 (t < 1.2 μs). The highest tempera-
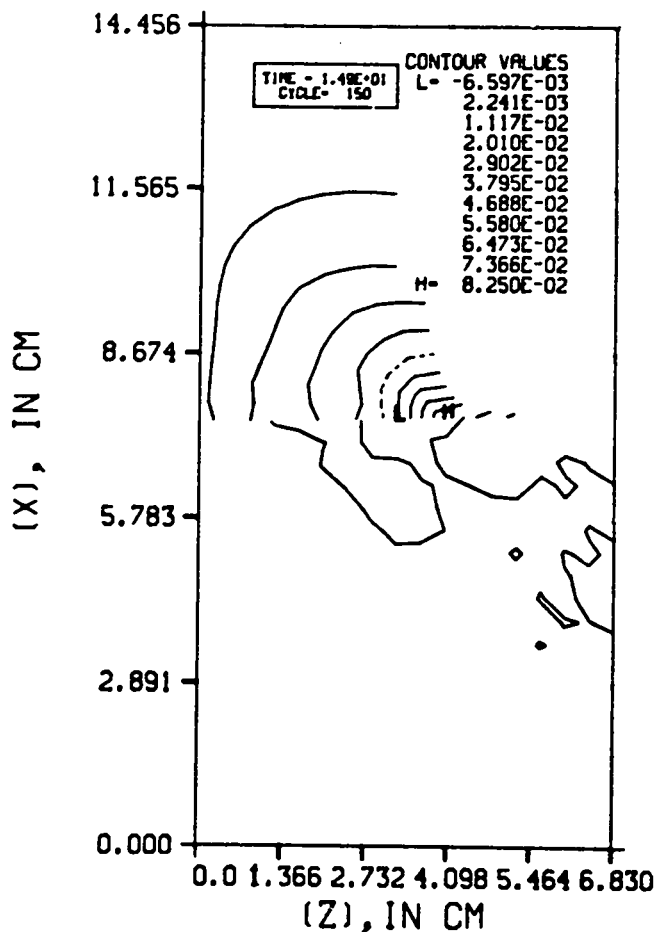ture in VRP is about 406 K near the
axis (Z = 0).

## Z-VELOCITY



Fig. AD-2.
Contours of radial velocity (cm/μs)
at 15 μs after impact for 70-mm gun,
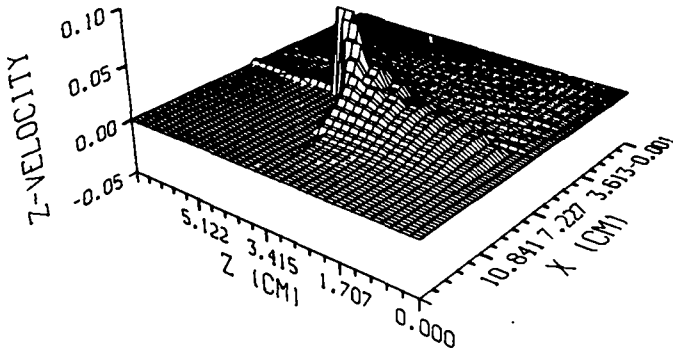calculated with cylindrical geometry
version of TDL code.

# Z-VELOCITY



TIME   1.4900E+01   CYCLE   150

Fig. AD-3.
Perspective plot of radial ve-
locity, 70-mm gun, t = 15 μs.
The side rarefaction in VRP is
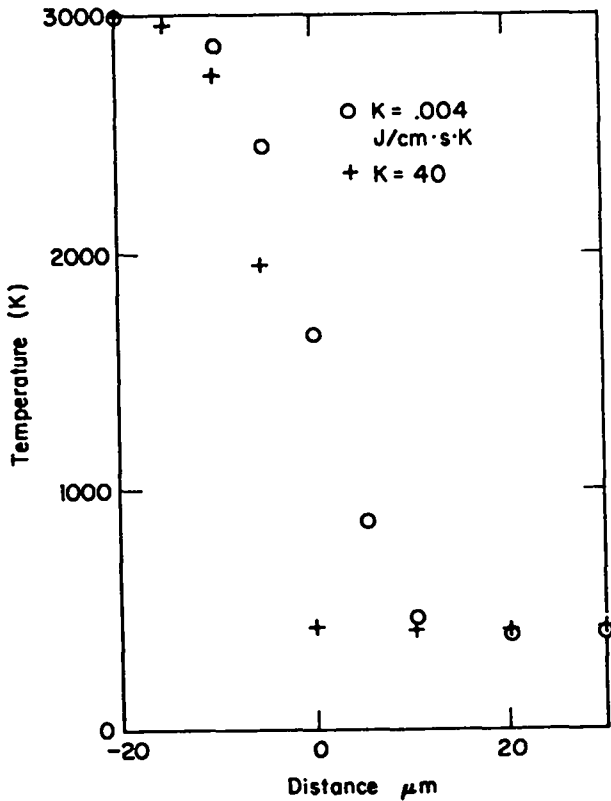conspicuous.



O K = .004
  J/cm·s·K
+ K = 40

Fig. AD-4.
The effect of enhanced thermal con-
ductivity on propagation of a temper-
ature wave into VRP. The circles
indicate the temperature profile at
100 μs after time of first zone burn,
calculated assuming the normal value
of K for unburned VRP (0 < x). The
other profile (+) was calculated as-
suming a conductivity for unburned
VRP arbitrarily enhanced by $10^4$.

# APPENDIX A

## FRICTION HEAT FLUX PARTITIONING AT INTERFACE BETWEEN MATERIALS WITH DIFFERENT THERMAL AND CONDUCTION PROPERTIES*

### I.   BOTH MATERIALS INITIALLY AT ZERO TEMPERATURE (Fig. A-1)

Let the time-dependence of the interface temperature be $f(t)$ $(0 \leqq t)$, and the flux into material $\underline{i}$ be

$$\phi_i(0,t) = -\lambda_i\left(\frac{\partial T}{\partial x}\right)_{x=0} \quad , \quad (i = 1,2) \quad .$$

Straightforward application of Laplace transform (LT) methods to the heat conduction equation for the case of a material in $0 \leqq x$ with surface at $T(0,t) = f(t)$ gives for the LT of $\phi(t)$

$$\bar{\phi}(0,s) = a_i^{-1} \mathcal{L}[f'(t)]\mathcal{L}[(\pi t)^{-1/2}] \quad .$$

---

*The first part of this appendix is based on a 1979 informal report by J. N. Johnson, Los Alamos National Laboratory.
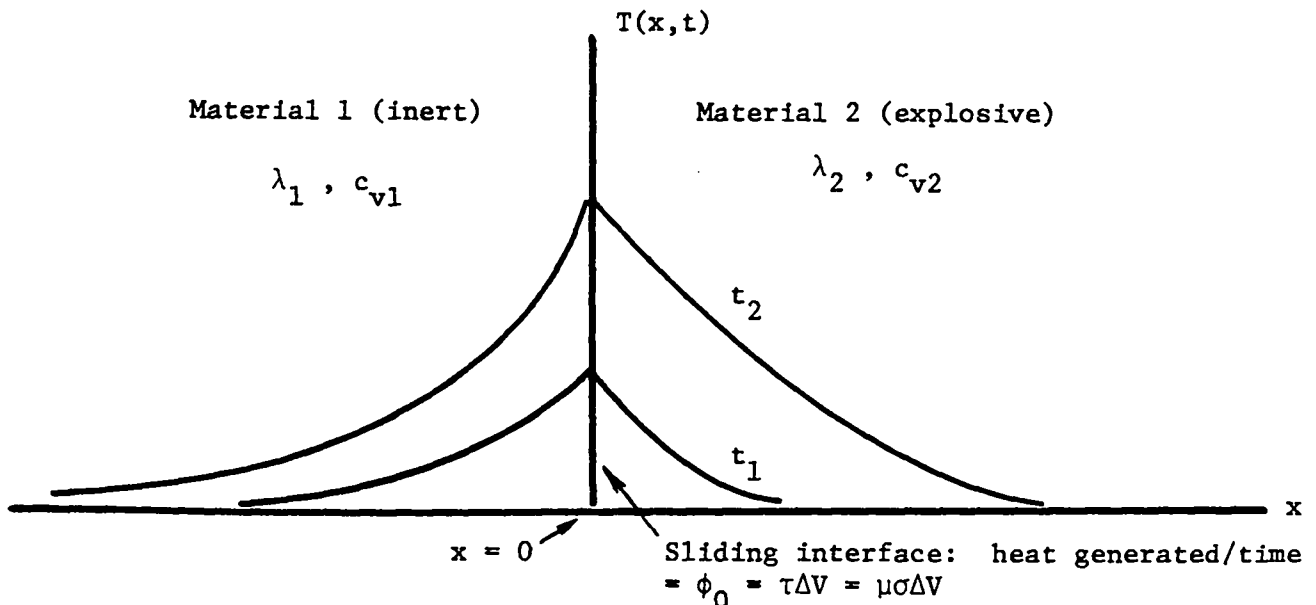


Fig. A-1.
Solution for both materials initially at zero temperature.

By the convolution theorem,

$$\phi(0,t) = a_i^{-1} \int_0^t (\pi t)^{-1/2} f'(t - \tau) d\tau \quad ;$$

that is, $a_i \phi(0,t)$ is a function only of the temperature history at $x = 0$. $a_i = (\rho_i c_{vi} \lambda_i)^{-1/2}$. Thus, if two thermally dissimilar materials are placed in contact so that the temperatures are equal at $x = 0$ and the total flux from the friction source is $\phi_0$ (assumed constant), then

$$-a_1 \phi_1(0,t) = a_2 \phi_2(0,t) \quad ,$$

and

$$-\phi_1(0,t) + \phi_2(0,t) = \phi_0 \quad .$$

The minus signs appear because the $\phi_i$ are algebraic quantities; that is, $\phi_1 < 0$ and $0 < \phi_2$. The preceding equations can be solved for $\phi_1, \phi_2$:

$$\phi_1(0,t) = -\frac{a_2}{a_1 + a_2} \quad , \quad \phi_0 = -(1 - f)\phi_0 \quad ,$$

$$\phi_2(0,t) = \frac{a_1}{a_1 + a_2} \quad , \quad \phi_0 \equiv f\phi_0 \quad .$$

This gives the flux partitioning at the interface. In the case of steel/VRP, the fraction $\underline{f}$ into VRP is ~0.07.

## II. TWO MATERIALS INITIALLY AT DIFFERENT TEMPERATURES

The solution is given by adding to the solution above, the solution for the case where the two materials have temperatures $T_0^-(x < 0)$ and $T_0^+(0 < x)$ with no heat source at the interface (Fig. A-2). Using LT techniques, the solution gives a contribution
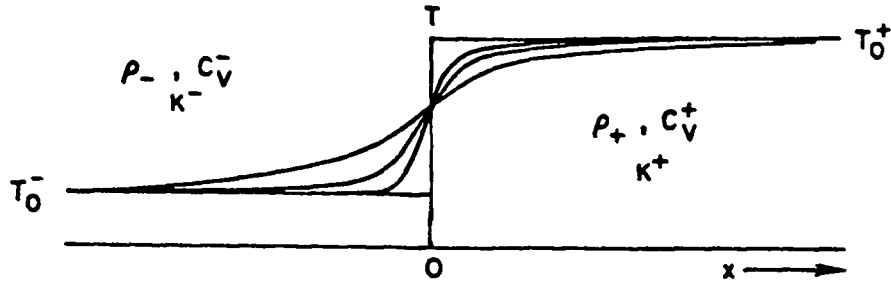
Fig. A-2.
Partial solution for two materials initially at different
temperatures.

$$\phi_{II}(0,t) = -\pi^{-1/2} \frac{\gamma_+ \gamma_-}{\gamma_+ + \gamma_-} (T_0^+ - T_0^-) t^{-1/2} \quad ,$$

where

$$\gamma_i = (\rho_i c_{vi} \lambda_i)^{1/2} \quad .$$

In the case of VRP impacting steel, this gives

$$\phi_{II}(0,t) = \left(-0.55 \times 10^{-9} \frac{\text{Mbar} \cdot \text{cm}^3}{\text{cm}^2 \cdot \text{K} \cdot \mu s^{1/2}}\right) (T_0^+ - T_0^-) t^{-1/2} \quad ,$$

which is a contribution directed from the VRP into steel because the initial
shock heating in steel (~314 K for an impact velocity of 0.05 cm/μs) is less
than in VRP (~410 K). That is, $\phi_{II}$ should be added to $\phi_1$ (steel) and subtracted
from $\sigma_2$(VRP). This contribution is significant only at early times; compare the
friction heat fluxes in Table III.

## APPENDIX B

CONTINUATION OF NUMERICAL HEAT FLOW SOLUTION BY APPROXIMATE ANALYTICAL TECHNIQUE

The temperature profile in the Shotgun 1-D numerical simulation at the time
that the first VRP zone burns is approximately as shown in Fig. B-1. The
first VRP zone extends from $x = 0$ to $x = x_1 \cong 2\Delta x_0$. $\Delta x_0$ = initial numerical
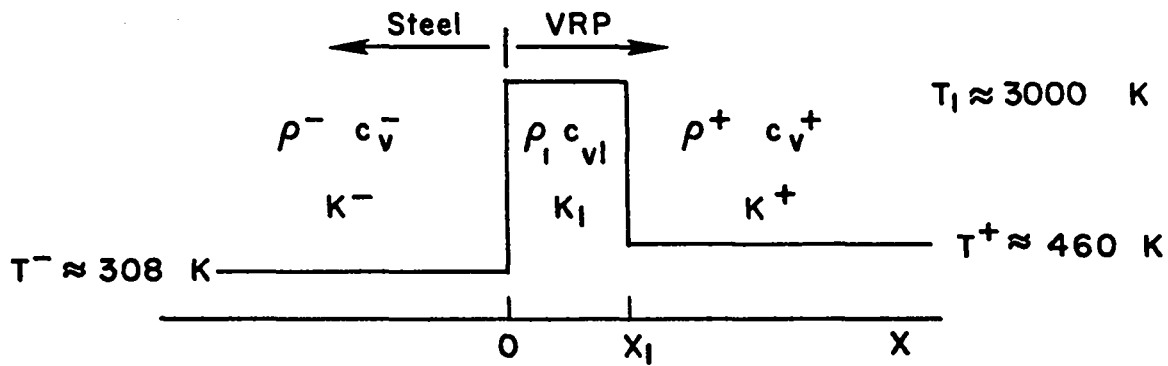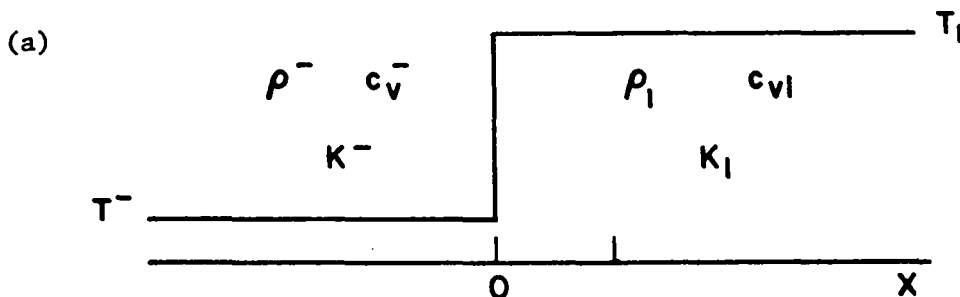
Fig. B-1
Shotgun Temperature profile.

integration zone size in VRP. The zone consists of burn products (mainly $N_2$, $H_2O$, C) at about 3000 K. $\rho_1 \cong 0.5\rho^+ \cong 0.5\rho_0$ (VRP). The parameters are
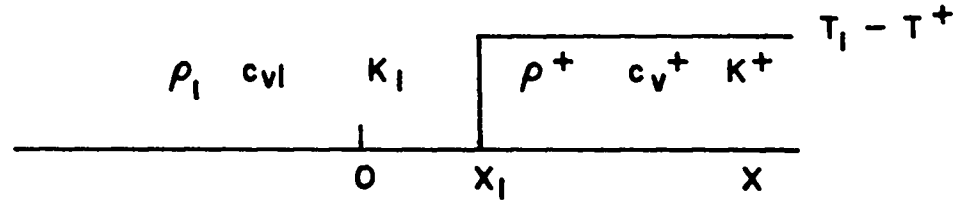
$$\rho^- = 8.1 \text{ g/cm}^3 \qquad \rho_1 \approx 1 \text{ g/cm}^3 \qquad \rho^+ \approx 2.2 \text{ g/cm}^3$$

$$c_v^- = 0.107 \qquad c_{v1} \approx 0.5 \qquad c_v^+ \approx 0.3 \text{ cal/g·K}$$

$$K^- = 0.1 \qquad K_1 \approx 0.001 \qquad K^+ \approx 0.001 \text{ cal/cm·s·K}$$

Extrapolation of thermal conductivity measurements for steam/$N_2$ mixture given by Touloukian et al.[5] to 3000 K gives a value within 25% of the value $K^+$ used for unburned VRP. The solution of the heat flow problem after this time is not very sensitive to material density variations, which, in any case, are not greater than about 15% in unburned VRP (see comment 5 below). The temperature versus time is particularly interesting in the second VRP zone after the time when the first zone burns.

An approximate analytical solution of the heat flow problem, with initial conditions as shown in Fig. B-1, is obtained by superposition (difference) of the solutions of two simpler problems with initial conditions as in (a) and (b) (approximation 1).

(b)

$$\rho_1 \quad c_{v1} \quad K_1 \qquad \rho^+ \quad c_v^+ \quad K^+ \qquad T_1 - T^+$$

$$0 \qquad x_1 \qquad \qquad x$$

That is, $T_{(1)}(x,t) = T_a(x,t) - T_b(x,t)$, where

$$T_a(x,t) = \begin{cases} T^- + \dfrac{\gamma_1}{\gamma_- + \gamma_1}\,(T_1 - T^-)\,\mathrm{erfc}\left[-\dfrac{1}{2}\left(\dfrac{\rho^- c_v^-}{K^- t}\right)^{1/2} x\right] & (x < 0) \\[4mm] T_1 - \dfrac{\gamma_-}{\gamma_- + \gamma_1}\,(T_1 - T^-)\,\mathrm{erfc}\left[\dfrac{1}{2}\left(\dfrac{\rho_1 c_{v1}}{K_1 t}\right)^{1/2} x\right] & (0 < x) \end{cases} ,$$

$$T_b(x,t) = \begin{cases} 0 + \dfrac{\gamma_+}{\gamma_1 + \gamma_+}\,(T_1 - T^+)\,\mathrm{erfc}\left[-\dfrac{1}{2}\left(\dfrac{\rho_1 c_{v1}}{K_1 t}\right)^{1/2} (x - x_1)\right] & (x < x_1) \\[4mm] T_1 - T_+ - \dfrac{\gamma_1}{\gamma_1 + \gamma_+}\,(T_1 - T^+)\,\mathrm{erfc}\left[\dfrac{1}{2}\left(\dfrac{\rho^+ c_v^+}{K^+ t}\right)^{1/2} (x - x_1)\right] & (x_1 < x) \end{cases} ,$$

in which expressions $\gamma \equiv (\rho c_v K)^{1/2}$ and erfc = error function complement. It is readily verified that $T_a$ and $T_b$ satisfy the heat conduction equation
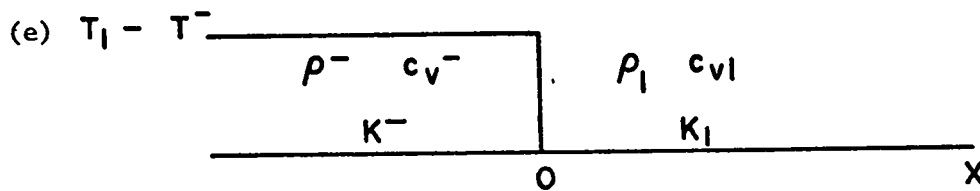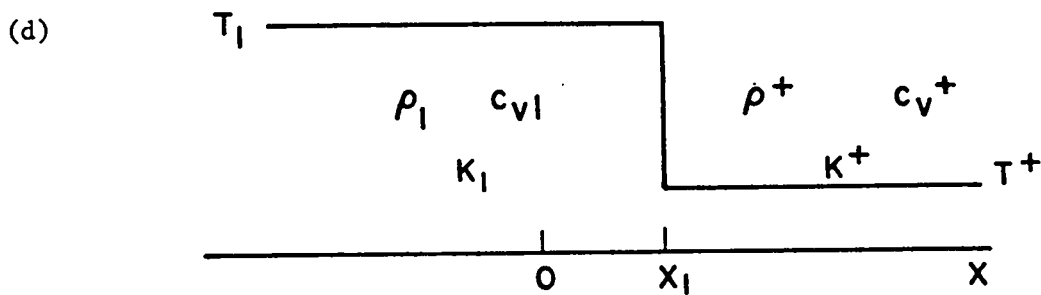
$$\rho c_v \frac{\partial T}{\partial t} = \frac{\partial}{\partial x} K \frac{\partial T}{\partial x}$$

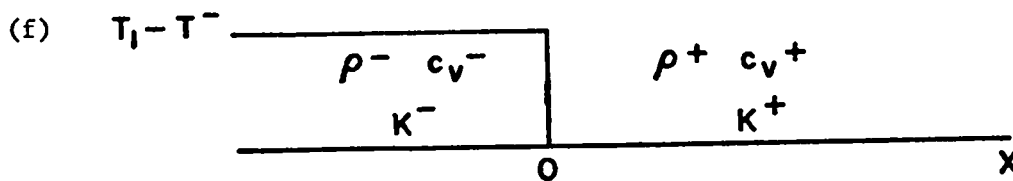and the initial conditions (a) and (b), respectively.

A different approximate solution (approximation 2) is given by $T_2(x,t) = T_c(x,t) - T_b(x,t)$, where $T_c(x,t)$ is given by expressions similar to those for $T_a$ above, with $\rho_1$, $c_{v1}$, $K_1$, $\gamma_1$ replaced by $\rho^+$, $c_v^+$, $K^+$, $\gamma^+$.

(c)

$\rho^- \quad c_v^-$

$K^-$

$\rho^+ \quad c_v^+$

$K^+$

$T^-$

$T_I$

0

X
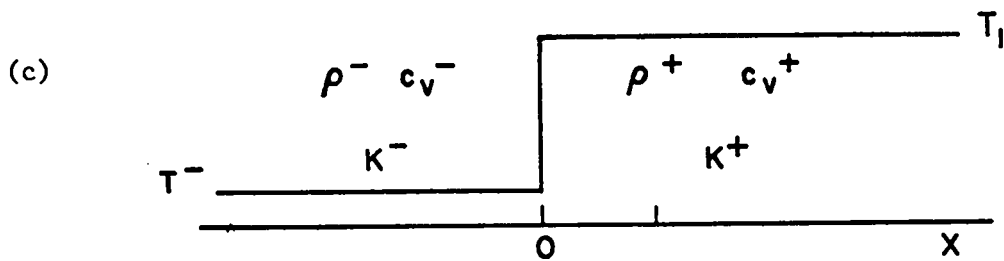
Other approximate solutions are $T_3x,t) = T_d(x,t) - T_e(x,t)$

(d)

$T_I$

$\rho_I \quad c_{vI}$

$K_I$

$\rho^+ \quad c_v^+$

$K^+$

$T^+$

0

$X_I$

X

(e) $T_I - T^-$

$\rho^- \quad c_v^-$

$K^-$

$\rho_I \quad c_{vI}$

$K_I$

0

X

and $T_{(4)}(x,t) = T_d(x,t) - T_f(x,t)$

(f) $T_I - T^-$

$\rho^- \quad c_v^-$

$K^-$

$\rho^+ \quad c_v^+$

$K^+$

0

X

are equivalent to approximations 1 and 2, respectively.  These were used as checks on the computations.

Figures 3 and 5 show temperature histories of the first two VRP zones for two different numerical integrations of the 1-D slab geometry, elastic-plastic flow equations, carried out with different initial $\Delta x$ [$\Delta x_0 = 0.001$ cm (1D-1) and $\Delta x_0 = 10^{-5}$ cm (1D-2)], up until the time at which the first VRP zone burns. Problem 1D-2 also included numerical integration of the heat conduction equation. Both problems included the same constant friction heat flux source at the steel/VRP interface obtained from a coarsely zoned 2-D calculation. The values of the parameters given above were obtained from the 1-D calculations. Problem 1D-1 was terminated at t = 1.45 μs because it did not include heat conduction, which is an important effect after the first zone burns. Although problem 1D-2 had heat conduction, it too was terminated just after the first zone burned, because the shock propagating into VRP associated with the expansion of the first zone at time of burn had run through all the zones available.

The approximate analytical solutions of the heat conduction equation given above were computed to extend the numerical calculations results, in particular to determine whether the second VRP zone is heated to ignition temperature (750-800 K). Results given in Figs. 6-8, B-2, and B-3[*] indicate that the temperature of the center of the second zone rises steadily, reaching 800 K after $\cong 80$ μs (problem 1D-1) and 0.01 μs (problem 1D-2). Until these times, approximations 1 and 2 give essentially the same result.

Although the combination of numerical integration and approximate analytical solutions may not constitute exact inductive proof, it suggests that when expansion cooling is neglected (comment 6 below), the friction-induced burn reaction propagates into a semi-infinite slab with velocity $\cong (0.01$ cm/x$)$ cm/s. On the other hand, the time scales indicate that during times of interest only very thin layers of VRP will burn by the hypothesized Arrhenius burn mechanism.

COMMENTS

(1) The true temperature profile is not a step function as in Fig. 1. The step function represents the result of zoned calculation.

(2) The assumed initial temperature profile (Fig. 1) neglects the heating of the first steel zone (adjacent to VRP), which is at substantial temperature

---

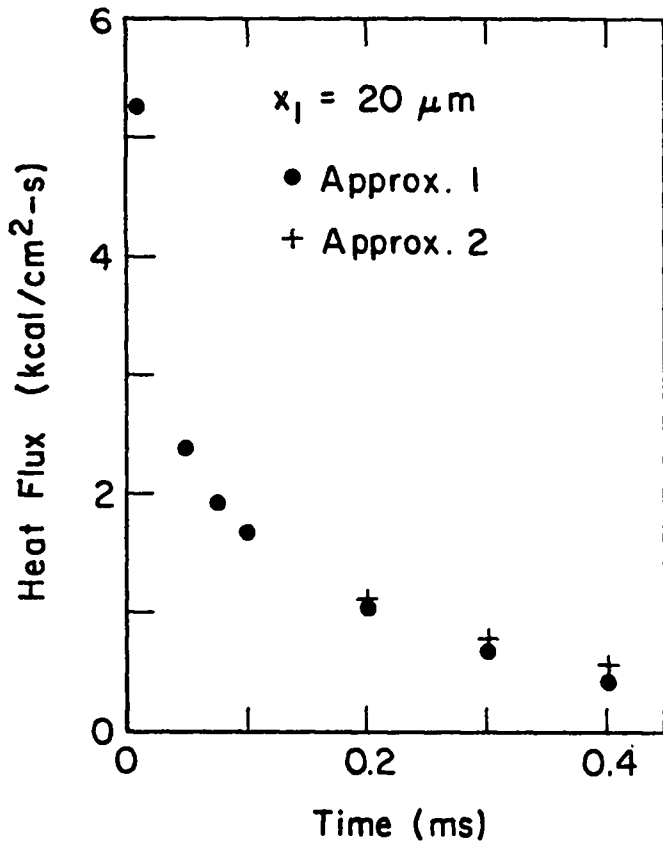[*]The zero of the time scales corresponds to the time at which the first zone burns.

Fig. B-2.
Heat flux from first to second VRP zone, problem 1D-1, as given by two different approximate analytical solutions.
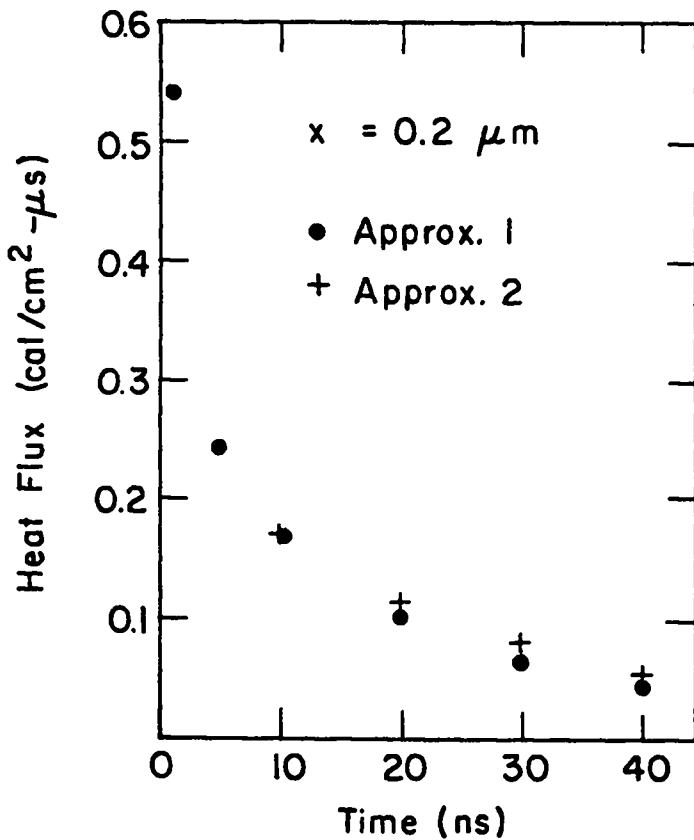


Fig. B-3.
Heat flux from first to second VRP zones, problem 1D-2, as given by two different approximate analytical solutions.

[$\cong 2400$ K (1D-1), $\cong 1100$ K(1D-2)]. Thus the analytical solution is conservative; that is, it overestimates the cooling rate of the burned VRP zone and the time to ignition of the second zone. Here we noted that $T_d(2.5 \times 10^{-5}$ cm,t) is practically indistinguishable from T2(2.5 x $10^{-5}$ cm, t) for t $\leqq$ 0.2 $\mu$s (1D-2). The value used for $T^+$ in problem II (393 K) should have been $\cong 430$ K = temperature behind second shock moving into VRP, again causing an error on the conservative side.

(3) The first VRP zone expanded only about 11% before it burned; thus the assumption of constant $\rho^+$ appears justified.

(4) At early times the flux at $x_1$, $F(x_1,t) \sim t^{-1/2}$ (see Figs. B-2 and B-3). The largest (absolute value) heat flux that can represented by a zoned numerical integration is K $(\Delta T/\Delta x) \cong 10^{-3}$ (3000 - 450)/$\Delta x) \sim 2500$ cal/cm$^2$ s (1D-1) and 0.25 cal/cm$^2$ $\mu$s (1D-2). The plots of $F(x_1,t$ reveal that the flux at early times after burn will be significantly underestimated in zoned calculations. This probably explains why the temperature versus time curve for the second VRP zone in Fig. 5 appears to be leveling off at 0.02 $\mu$s < t.

(5) To investigate the sensitivity of the solutions to density variations, problem 1D-2 was also run in approximation 1 with $\rho^+$ arbitrarily increased by 10%. The temperature versus time curve for the center of the second VRP zone T (2.5 x $10^{-5}$ cm, t) is within 5% of the curve with $\rho^*$ unchanged.

(6) The analytical solution of the heat flow equation neglects expansion cooling, $c_v^{-1}p\partial V/\partial t$. Figures B-4 and B-5 show this quantity and the net heating rate for the first (1D-1) and first two (1D-2) VRP zones, from the zoned hydro calculations. In these cases the expansion cooling rates are about 20% of the heating rates. In the 2-D case there will also be expansion cooling associated with side rarefactions (Table IV).
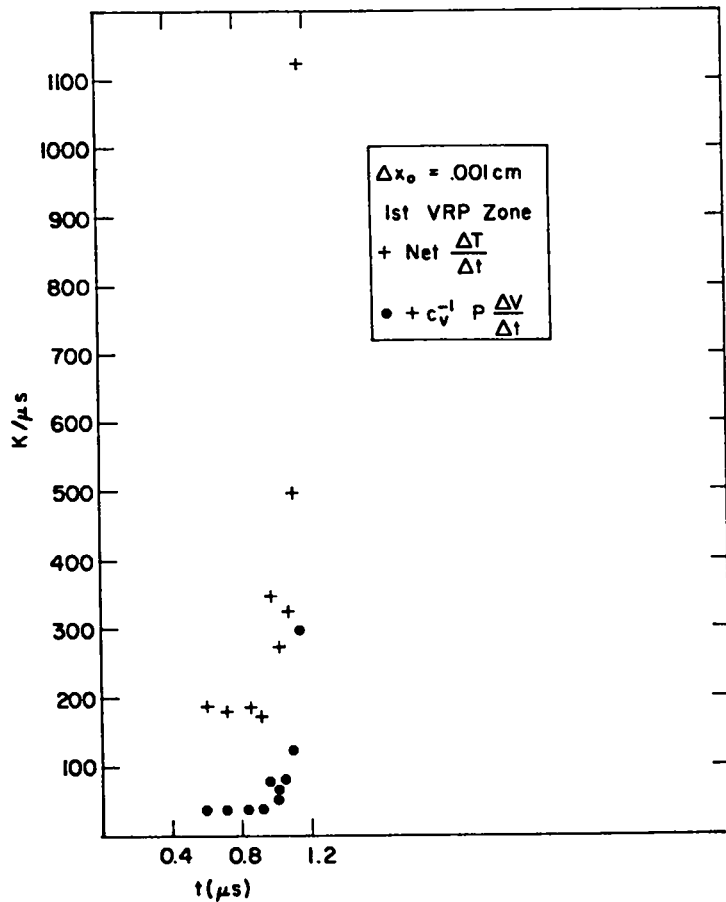
Fig. B-4.
Net heating rate $\Delta T/\Delta t$ and expansion cooling rate $(c_v^{-1}P\Delta V/\Delta t)$ for first VRP zone, problem 1D-1, from zoned calculation.
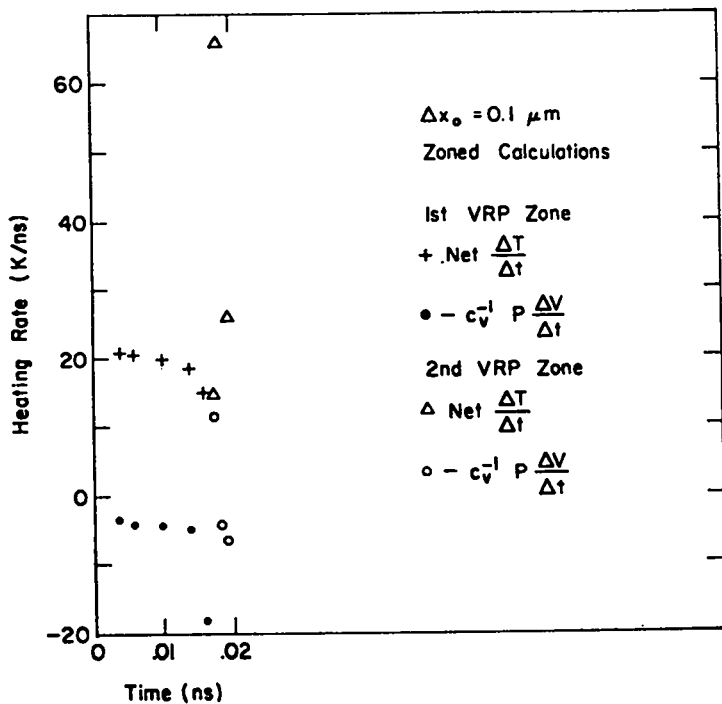


Fig. B-5.
Net heating and expansion cooling rates for first and second VRP zones, problem 1D-2, from zoned calculation.

REFERENCES

1. C. L. Mader, <u>Numerical Modeling of Detonations</u> (University of California Press, Berkeley, 1979).

2. W. H. Anderson, Propellants Explos. <u>6</u>, 17-23 (1981).

3. F. P. Bowden and D. Tabor, <u>The Friction and Lubrication of Solids</u> (Oxford Press, 1950), Vol. I, Plate I.

4. D. D. Bloomquist and S. A. Sheffield, "Thermocouple Temperature Measurements in Shock Initiated PBX 9404," Seventh Symposium (International) on Detonation, Annapolis, Maryland, June 16-19, 1981, Vol. 2, p. 829.

5. Y. S. Touloukian, P. E. Liley, and S. C. Saxena, Eds., <u>Thermophysical Properties of Matter, Vol. 3, Thermal Conductivity: Nonmetallic Liquids and Gases</u> (Plenum Press, New York, 1970).

| Page Range | Domestic Price | NTIS Price Code | Page Range | Domestic Price | NTIS Price Code | Page Range | Domestic Price | NTIS Price Code | Page Range | Domestic Price | NTIS Price Code |
|---|---|---|---|---|---|---|---|---|---|---|---|
| 001-025 | $ 5.00 | A02 | 151-175 | $11.00 | A08 | 301-325 | $17.00 | A14 | 451-475 | $23.00 | A20 |
| 026-050 | 6.00 | A03 | 176-200 | 12.00 | A09 | 326-350 | 18.00 | A15 | 476-500 | 24.00 | A21 |
| 051-075 | 7.00 | A04 | 201-225 | 13.00 | A10 | 351-375 | 19.00 | A16 | 501-525 | 25.00 | A22 |
| 076-100 | 8.00 | A05 | 226-250 | 14.00 | A11 | 376-400 | 20.00 | A17 | 526-550 | 26.00 | A23 |
| 101-125 | 9.00 | A06 | 251-275 | 15.00 | A12 | 401-425 | 21.00 | A18 | 551-575 | 27.00 | A24 |
| 126-150 | 10.00 | A07 | 276-300 | 16.00 | A13 | 426-450 | 22.00 | A19 | 576-600 | 28.00 | A25 |
| | | | | | | | | | 601-up | † | A99 |

†Add $1.00 for each additional 25-page increment or portion thereof from 601 pages up.

Los Alamos